Sustainable Energy & Fuels

ROYAL SOCIETY OF CHEMISTRY

PAPER

View Article Online
View Journal

Cite this: DOI: 10.1039/d6se00061d

Light-driven hydrogen evolution reactivity of molecular thio-oxomolybdate catalysts

Luca T. Schleicher,†[a] S. Henriette Kolbinger,†[a] Akuila Edwards,[b] Kristin Sellmann,[a] Luis Senz,[a] Stephan Kupfer,[b] Michael Schmitt,[b] Jürgen Popp *[bc] and Carsten Streb *[a]

Received 16th January 2026
Accepted 5th April 2026

DOI: 10.1039/d6se00061d

rsc.li/sustainable-energy

Heterogeneous molybdenum sulfides are widely used noble metal-free hydrogen evolution reaction (HER) catalysts. Thiomolybdates, their molecular analogues have been developed as viable minimal models to study reactivity at the molecular level. Here, we explore the light-driven HER reactivity and stability of the mixed thio-oxo-molybdate prototype $[Mo_2O_2S_6]^{2-}$ in homogeneous solution. In combination with the photosensitizer $[Ru(bpy)_3]^{2+}$, $[Mo_2O_2S_6]^{2-}$ shows promising HER performance (turnover number TON > 500), as well as strong reactivity dependence on the reaction conditions. Mechanistic experimental studies combined with density functional theory computations reveal complex speciation of the catalyst in solution, as well as light-induced and light-independent reaction pathways for catalyst and photosensitizer which are in line with disulfide-for-solvent ligand exchange reactions. These structure–reactivity insights outline design rules for more robust, solvent-tolerant thiomolybdate HER catalysts.

Motivation & introduction

The development of sustainable catalysts for green hydrogen production is a major global research goal. Molybdenum sulfides have emerged as promising candidates for the hydrogen evolution reaction (HER), since they are earth-abundant and noble-metal-free.[1–5] Molecular molybdenum sulfides, so-called thiomolybdates are ideal models to rationalize HER reactivity and have been investigated as homogeneous and heterogenized catalysts for photochemical and electrochemical HER.[6–11] The prototype thiomolybdate cluster $[Mo_3S_{13}]^{2-}$ (Fig. 1) is the most studied system to-date. When operated in homogeneous MeOH : H_2O solution in combination with $[Ru(bpy)_3]^{2+}$ as photosensitizer (PS) and ascorbic acid as electron/proton donor, TONs >20 000 have been achieved after 6 h of visible light-irradiation.[7] Note that the catalytic performance depends strongly on the reaction conditions including solvent, reagent concentrations and sample preparation. Concerning solvent dependent performance, a mixture of methanol and water (10 : 1, v/v) was found to be optimal in terms of TON and TOF.[7] Experimental and theoretical mechanistic studies revealed that under reaction conditions (in a MeOH : H_2O mixture (1 : 1, v/v)), $[Mo_3S_{13}]^{2-}$ undergoes substitution of terminal disulfide ligands for solvent ligands L (L = MeOH, H_2O) on a timescale of less than one hour.[7] These studies also showed that partially ligand-exchanged species featured higher HER-catalytic activity than the native catalyst, while full exchange of all three terminal disulfide ligands leads to a species with low HER-activity.[7] More recent studies suggest that ligand exchange is accelerated upon irradiation with visible light.[12] These dynamic effects and complex (light-induced) speciation equilibria make mechanistic studies challenging. Similar observations on solvent-dependent HER-activity were made for the thiomolybdate $[Mo_2S_{12}]^{2-}$ (Fig. 1): highest HER-activity was observed in pure methanol, and when combined with the PS $[Ru(bpy)_3]^{2+}$ and ascorbic acid as electron/proton donor, TONs >1500 were observed.[6] Here, Raman spectroscopy revealed that ligand exchange occurs on a much slower timescale (>12 h) compared with $[Mo_3S_{13}]^{2-}$ indicating that the cluster structure significantly affects ligand-exchange and HER reactivity.[6] Inspired by these studies, we hypothesized that structure modification on the Mo_2-framework could have significant impact on HER activity. To this end, this study reports the first experimental and theoretical insights into the homogeneous, light-driven HER reactivity of thio-oxo-molybdates. Thio-oxo-molybdates are structurally related to thiomolybdates and have so far received little attention, despite their potential as noble metal-free HER catalysts where reactivity can be tuned by modification of the oxo-to-(di)sulfide ligand environment.[13,14] Keita *et al.* reported that a mixed thio-oxo-molybdates based on $[Mo_2O_2S_2]^{2+}$ building blocks can be used as efficient electrocatalysts for the HER.[15] In an exemplary

[a]Department of Chemistry, Johannes Gutenberg-University, Duesbergweg 10-14, 55128 Mainz, Germany. E-mail: carsten.streb@uni-mainz.de

[b]Institute of Physical Chemistry and Abbe Center of Photonics, Friedrich-Schiller University Jena, Helmholzweg 4, 07743 Jena, Germany. E-mail: juergen.popp@uni-jena.de

[c]Leibniz Institute of Photonic Technology, Albert-Einstein-Straße 9, 07745 Jena, Germany

† These authors contributed equally.

study, Miras and co-workers showed that the thio-oxo-molybdate $[Mo_2O_2S_6]^{2-}$ (Fig. 1) features significant electrocatalytic HER activity.[16] Briefly, $[Mo_2O_2S_6]^{2-}$ is composed of two Mo(v) centers are linked by two bridging sulfides (μ-S^{2-}). Each metal center is additionally coordinated by one terminal disulfide ligand (η^2-S_2^{2-}) and one terminal oxo ligand. In contrast, the pure thiomolybdate $[Mo_2S_{12}]^{2-}$ is based on two Mo(v) linked by two bridging disulfide ligands (μ-S_2^{2-}). Each Mo also features two terminal disulfide ligands (Fig. 1). To-date, there is virtually no information on the behavior of thio-oxo-molybdates such as $[Mo_2O_2S_6]^{2-}$ under light-driven homogeneous HER catalytic conditions.

Previous investigations have utilised density functional theory (DFT) calculations to study the HER energetics for $[Mo_3S_{13}]^{2-}$, $[Mo_2S_{12}]^{2-}$ and $[Mo_2O_2S_6]^{2-}$.[7,16,17] These studies suggested a Volmer–Heyrovsky-type mechanism as energetically most favourable for all three catalysts. In the case of $[Mo_3S_{13}]^{2-}$ and $[Mo_2S_{12}]^{2-}$, calculations have shown the sulfur-centered mechanism, involving one of the bridging disulfide ligands as active site to be energetically favoured.[7,17] However, in $[Mo_2O_2S_6]^{2-}$, where no bridging disulfide is present, the active site is assumed to be a terminal disulfide ligand which presumably undergoes a proton-coupled reductive (reversible) cleavage of the S–S bond, resulting in the formation of a protonated sulfide as reactive intermediate.[16] In sum, research on thio(oxo)molybdate has demonstrated that changes to the ligand environment of these species have major effects on stability and HER-reactivity.

The present study takes inspiration from these studies and aims to address knowledge gaps regarding the light-driven homogeneous HER activity of the thio-oxo-molybdate $[Mo_2O_2S_6]^{2-}$. Based on catalytic studies, *in situ* Raman spectroscopy and quantum chemical calculations at the DFT level of theory, we provide understanding into HER activity, plausible reaction pathways and the impact of ligand exchange on this cluster prototype, thereby guiding future catalyst development efforts.

Results and discussion

Initially, we explored the homogeneous HER activity of $[Mo_2O_2S_6]^{2-}$ when used with $[Ru(bpy)_3]^{2+}$ as photosensitizer (PS) and ascorbic acid/ascorbate as sacrificial electron donor (SED) in homogeneous MeOH : H_2O mixtures, inspired by earlier studies on thiomolybdates.[6,7] Briefly, the thio-oxo-molybdate $(NMe_4)_2[Mo_2O_2S_6]$ was synthesized based on a reported method, for details see SI.[18]

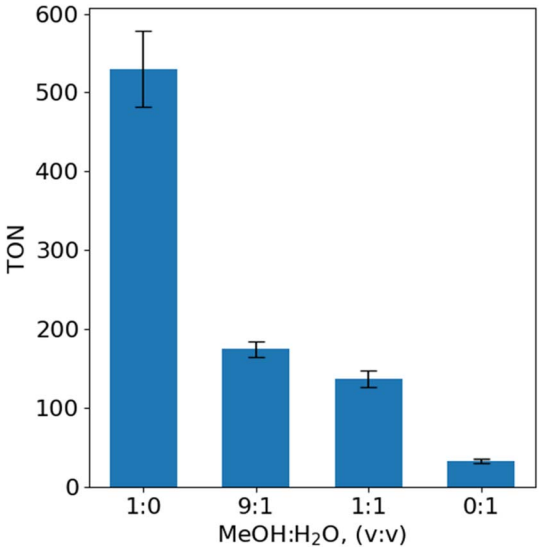

Fig. 2 TON of the $[Mo_2O_2S_6]^{2-}$ system in MeOH : H_2O solvent mixtures. Catalytic conditions: c($[Mo_2O_2S_6]^{2-}$) = 0.5 μM, c(PS) = 20 μM, c(SED) = 10 mM, pH 4.

The standard reaction setup contained $(NMe_4)_2[Mo_2O_2S_6]$ (0.5 μM), the PS, *i.e.*, $[Ru(bpy)_3](PF_6)_2$ (20 μM) and the sacrificial electron donor ascorbic acid/sodium ascorbate (buffered, aqueous solution, total concentration 10 mM, pH 4). First, we determined the solvent conditions under which $[Mo_2O_2S_6]^{2-}$ exhibits optimum light-driven HER performance. To this end, four different solvent ratios were tested: pure methanol, pure water and two MeOH : H_2O mixtures (9 : 1 and 1 : 1, v/v). These conditions are similar to those used in experiments performed for thiomolybdates.[6,7] All samples were irradiated for 300 min in a custom-built modular photoreactor[19] using LED irradiation (λ_{max} = 465 nm, P = 13 mW cm^{-2}, q = 51 nmol cm^{-2} s^{-1}). Hydrogen evolution was determined by using gas chromatography. Each experiment was carried out in triplicate, and the average turnover number and standard deviation were determined (see Fig. 2). Blank reference experiments performed in

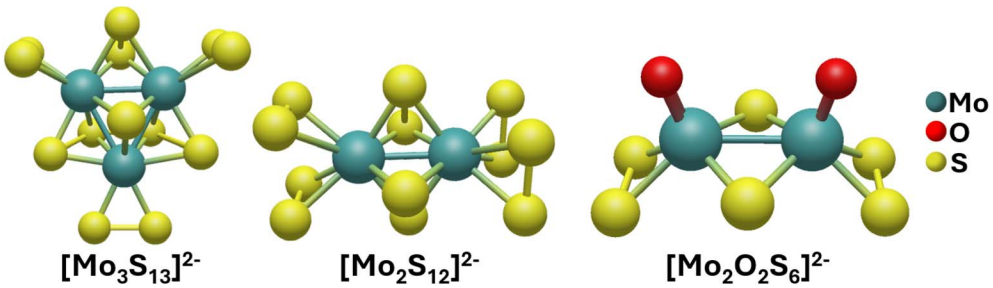

Fig. 1 Ball-and-stick representations of the molecular structure of the thiomolybdates $[Mo_3S_{13}]^{2-}$ (left), $[Mo_2S_{12}]^{2-}$ (centre) and the thio-oxo-molybdate $[Mo_2O_2S_6]^{2-}$.

the absence of the catalyst showed only low levels of hydrogen evolution (see SI, Table S2).

Fig. 2 illustrates the TONs obtained after 300 min irradiation. The data show that highest HER performance is observed in pure methanol (TON *ca.* 530). For comparison: reference experiments using $[Mo_3S_{13}]^{2-}$ as catalyst under similar conditions gave a TON of 670.[12] Increasing the water content leads to a continuous TON decrease, with the lowest activity observed in pure water (TON ≈ 33). This behavior is similar to the solvent-dependent HER performance of $[Mo_2S_{12}]^{2-}$.[6] One hypothesis to explain this behavior is the rapid degradation of the photosensitizer in aqueous solutions. In the 1 : 1 mixture and pure water, discoloration of the solution was observed upon irradiation, which might also be a reason for the lower catalytic activity of the system. The formation of $[Ru(bpy)_2(H_2O)_2]^{2+}$ in aqueous solutions has been previously reported in the literature.[20] PS degradation was further studied by monitoring changes of the characteristic PS MLCT absorption band (452 nm) using time-lapse UV-Vis spectroscopy. Here, we studied the impact of different solvent mixtures as well as presence/absence of catalyst on PS degradation (SI, Fig S8). Analysis of these data shows that PS degradation kinetics are not affected by the catalyst, and the rate of PS bleaching is dominantly controlled by the solvent composition. Higher water concentrations significantly increase PS degradation.

To determine whether ligand exchange processes occur for $[Mo_2O_2S_6]^{2-}$, time-resolved Raman spectroscopy was performed. Raman spectroscopy offers high molecular selectivity and can be applied *in situ* under catalytic conditions; however, the intrinsically low Raman scattering cross-section necessitates comparatively high analyte concentrations for sufficient signal-to-noise ratios. Accordingly, due to the low catalyst concentrations used in the light-driven HER experiments, Raman measurements were performed at elevated catalyst concentrations (2.5 mM). The Raman spectrum of $[Mo_2O_2S_6]^{2-}$ exhibits two characteristic vibrational bands, which were identified using DFT frequency calculations (see SI). The band at 530 cm^{-1} corresponds to vibrations of the bridging sulfide ligands, while the band at 560 cm^{-1} is assigned to the terminal disulfide ligands. Raman experiments were conducted in pure methanol, pure water and MeOH : H_2O (1 : 1, v/v). Representative Raman spectra recorded for the catalyst in pure methanol are shown in Fig. 3. The Raman data for the other solvent conditions are shown in the SI.

Monitoring the two characteristic Raman signals of $[Mo_2O_2S_6]^{2-}$ over a period of five hours revealed that the intensity of the 530 cm^{-1} band remains relatively stable, whereas the 560 cm^{-1} band shows a steady decrease in intensity. This trend indicates that under the given reaction conditions, the terminal disulfide ligands undergo exchange for solvent molecules. Also, comparison of the different solvent conditions revealed that the decay rates are of the same order of magnitude ($\approx 10^{-2}$ min^{-1}), suggesting that ligand exchange is not strongly solvent-dependent and occurs at similar rates in methanol and water. It cannot be excluded that under catalytic conditions at lower optical densities and with active photosensitizer present, photochemical processes may contribute differently.

To further corroborate these findings, and to study the impact of irradiation on the proposed MeOH for disulfide ligand exchange, we performed time-lapse UV-Vis-spectroscopy. Here, we studied solutions of the catalyst in pure MeOH or MeOH : H_2O (1 : 1, v/v) for periods of 300 min under continuous LED irradiation at 465 nm. For both solvent conditions, we observe nearly identical spectral changes of the characteristic catalyst signals under irradiation, while the non-irradiated samples show no significant spectral changes (Fig. 3b, SI, S9–S11). In detail, for the measurements in methanol (Fig. 3b), we observe the loss of several characteristic peaks (270 nm, 375 nm, 470 nm), while two new signals (385 nm, 440 nm) emerge after 30 min of irradiation. Upon prolonged irradiation, these two signals continuously decrease and disappear after 300 min irradiation. This observation is in line with a two step-process, where first, the native catalyst is converted into an intermediate species which then undergoes a second conversion step. Note that for MeOH : H_2O (1 : 1, v/v) mixtures, we observe virtually identical UV-Vis signal changes, indicating a similar mechanism (SI, Fig. S9). In sum, Raman spectroscopy and UV-Vis-spectroscopy both indicate significant structural changes of $[Mo_2O_2S_6]^{2-}$ in solution. While Raman data indicate the replacement of terminal disulfide ligands on a 0–60 min timescale, UV-Vis spectroscopy indicates two processes on a 0–180 min timescale, resulting in changes of the electronic structure of the catalyst. This complex behaviour is in line with

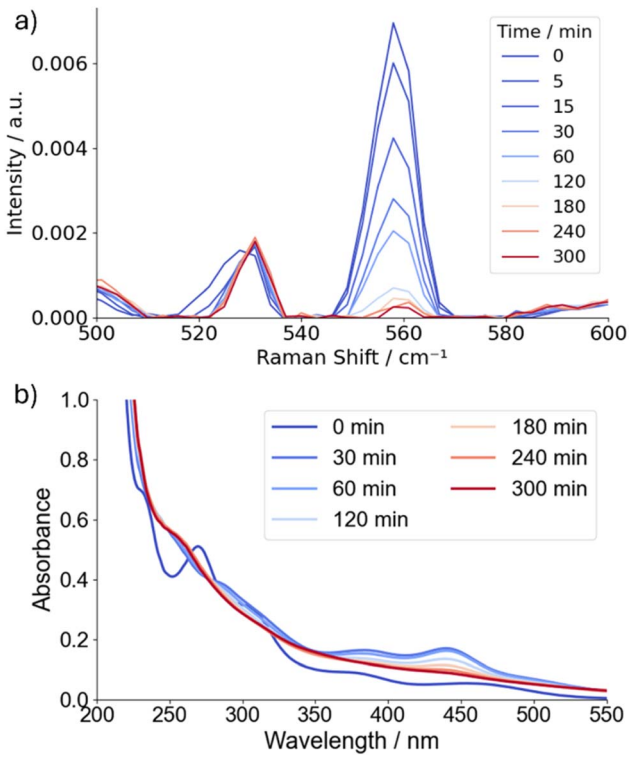

Fig. 3 (a) Time-dependent Raman spectra of $[Mo_2O_2S_6]^{2-}$ in MeOH (c = 2.5 mM). (b) Time-dependent UV-Vis spectra of $[Mo_2O_2S_6]^{2-}$ (c = 50 μM) in MeOH.

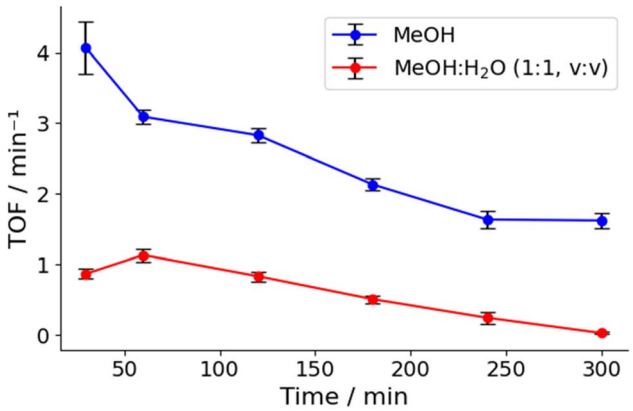

Fig. 4 TOF for the light-driven hydrogen evolution by $[Mo_2O_2S_6]^{2-}$ during 300 min irradiation in pure methanol as well as in MeOH : H_2O 1 : 1, v/v.

previous reports on thiomolybdate ligand exchange under irradiation.[7,12]

To further study the electrochemical behaviour of $[Mo_2O_2S_6]^{2-}$, we used cyclic voltammetry analyses. Measurements were performed in acetonitrile containing molar ratios of $[Mo_2O_2S_6]^{2-}$: MeOH ranging from 0 to 20 (SI, Section 2.9). As a general trend, we observe that increasing MeOH concentrations lead to changes of the CV signals of the catalyst: for the one-electron reduction process at −1.1 V, we observe a minor cathodic shift (<50 mV) upon methanol addition, which might be indicative of structural changes of the catalyst, or changes induced by the changing solvent compositions. Note that this reduction potential indicates that both oxidative quenching (E = −1.23 V) as well as reductive quenching (E = −1.72 V) of the catalyst by the photosensitizer is in principle feasible.[21] Also, we note the observation of an irreversible oxidation peak at approximately +1.1 V, which is assigned to oxidation of the cluster-bound disulfide ligands,[22] indicating that oxidative decomposition of the cluster occurs under these conditions.

Next, we analyzed the time-dependent turnover frequency (TOF) of HER catalysis to gain further understanding of the proposed structural changes and ligand exchange proposed for $[Mo_2O_2S_6]^{2-}$. Specifically, we studied the standard reaction systems using MeOH or MeOH : H2O (1 : 1) as solvents and monitored the hydrogen evolution over five hours using the standard catalytic system described in Fig. 2. The resulting TOF profiles are shown Fig. 4. The TOF data reveal two major trends. First, the overall catalytic activity is higher in pure methanol, consistent with the solvent-dependence observed for the TON (Fig. 2). Second, the TOF time-dependency differs between the two solvent systems: in the MeOH : H_2O mixture, the TOF shows a modest increase during the initial phase of the reaction, followed by a steady decrease at longer reaction times. This behavior is consistent with the stepwise formation of a catalytically more active species, followed by a second, subsequent deactivation. This is also in line with similar stepwise deactivation processes reported previously for $[Mo_3S_{13}]^{2-}$.[7] In contrast, in pure methanol, the maximum TOF is already reached at the earliest recorded data point (30 minutes), followed by continuous decrease of TOF. Note that due to experimental procedures, there is a delay of approximately 60 min between catalyst dissolution and the start of irradiation. This period provides sufficient time for initial ligand exchange before catalysis is initiated. Consequently, it cannot be excluded that a ligand-exchanged species, rather than the pristine $[Mo_2O_2S_6]^{2-}$ cluster, represents the catalytically active form present at the first data points under the given conditions. Also note that catalytic and Raman data can only qualitatively be compared since the systems were operated at different catalyst concentrations as described in the Raman section above. Also, differences in the observed kinetic behavior between pure methanol and the MeOH : H_2O mixture may also reflect differences in the equilibration dynamics of ligand exchange: in mixed solvents, the presence of multiple equilibria could lead to slower establishment of a catalytically relevant species. Furthermore, the dynamics of other mechanistic steps which may be solvent-dependent such as PS quenching by the electron donor, need to be taken into account, as these steps are also affected by the reaction conditions.[23] Nevertheless, overall, the kinetic observations support the notion that ligand substitution leads to the generation of distinct catalytic species with

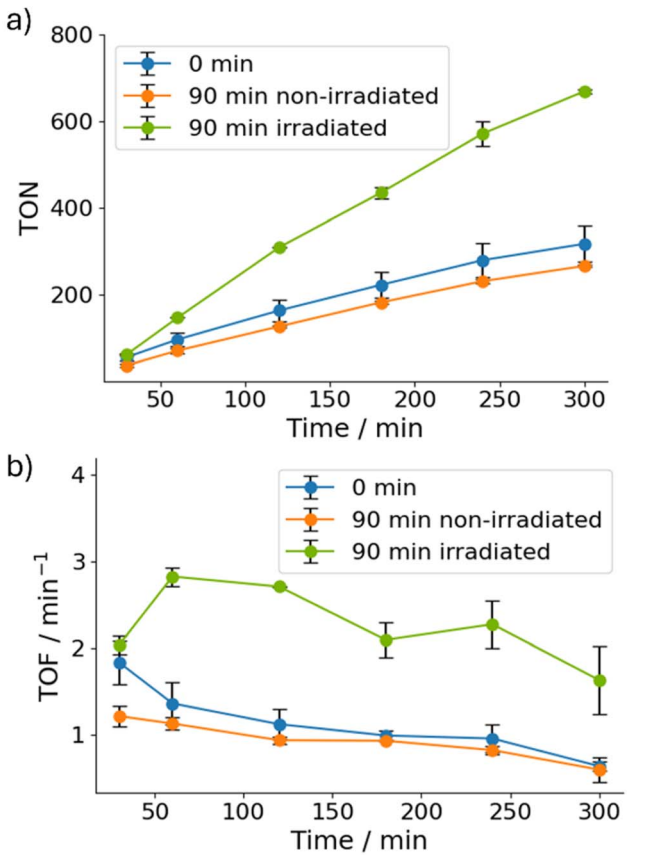

Fig. 5 (a) Time-dependent TON and (b) TOF for the photocatalytic system (c($[Mo_2O_2S_6]^{2-}$) = 0.5 μM, c(PS) = 20 μM, c(SED) = 10 mM, pH 4 in MeOH) for three different catalyst stock solutions: blue = freshly dissolved stock solution, orange = stock solution was left under non-irradiated conditions for 90 min, green = stock solution was irradiated for 90 min (λ = 465 nm).

different reactivity profiles. However, the data also show that in future work, more detailed, time-resolved *operando* studies are required to gain further molecular-level insights into this complex reaction system.

To provide further evidence for the underlying causes of structural changes to the catalytic system, we performed reference experiments which were kept under light or dark conditions: we studied three catalytic systems: (I), a freshly prepared catalyst stock solution ($[Mo_2O_2S_6]^{2-}$ (c = 0.5 mM) in MeOH) which was used immediately; (II) the same catalyst stock solution which was stored under inert conditions for 90 min under dark conditions: (III) the same catalyst stock solution which was stored under inert conditions while being irradiated with a 465 nm LED for 90 min. As shown in Fig. 5, we observe that for the irradiated solution, we observe significantly higher TONs compared to the two reference systems. These data further support our hypothesis that light-irradiation initiates structural changes to the catalyst which result in the (initial) formation of a more active HER catalyst species.[20] The findings are also in line with previous studies which reported similar activation/deactivation cascades for thiomolybdate HER catalysts.[7,16]

Quantum chemical analysis of catalytic activity

To rationalize the experimental observations and the apparent role of ligand substitution in catalytic activation, computational analysis of the catalytic activity was performed. Similar to investigations concerning $[Mo_3S_{13}]^{2-}$, DFT calculations (details see SI, Section 2.7) aimed to assess the thermodynamics of the various intermediates on the HER activity of $[Mo_2O_2S_6]^{2-}$.[7] Based on prior studies, the HER active sites are assumed to be the terminal disulfide ligands in $[Mo_2O_2S_6]^{2-}$.[5,16] Although a variety of different processes appear feasible during HER catalysis, the following key mechanisms involving the terminal disulfide ligands are primarily considered in the present study: proton-coupled electron transfer (PCET), electron transfer/reduction (ET), proton transfer (PT), and finally hydrogen

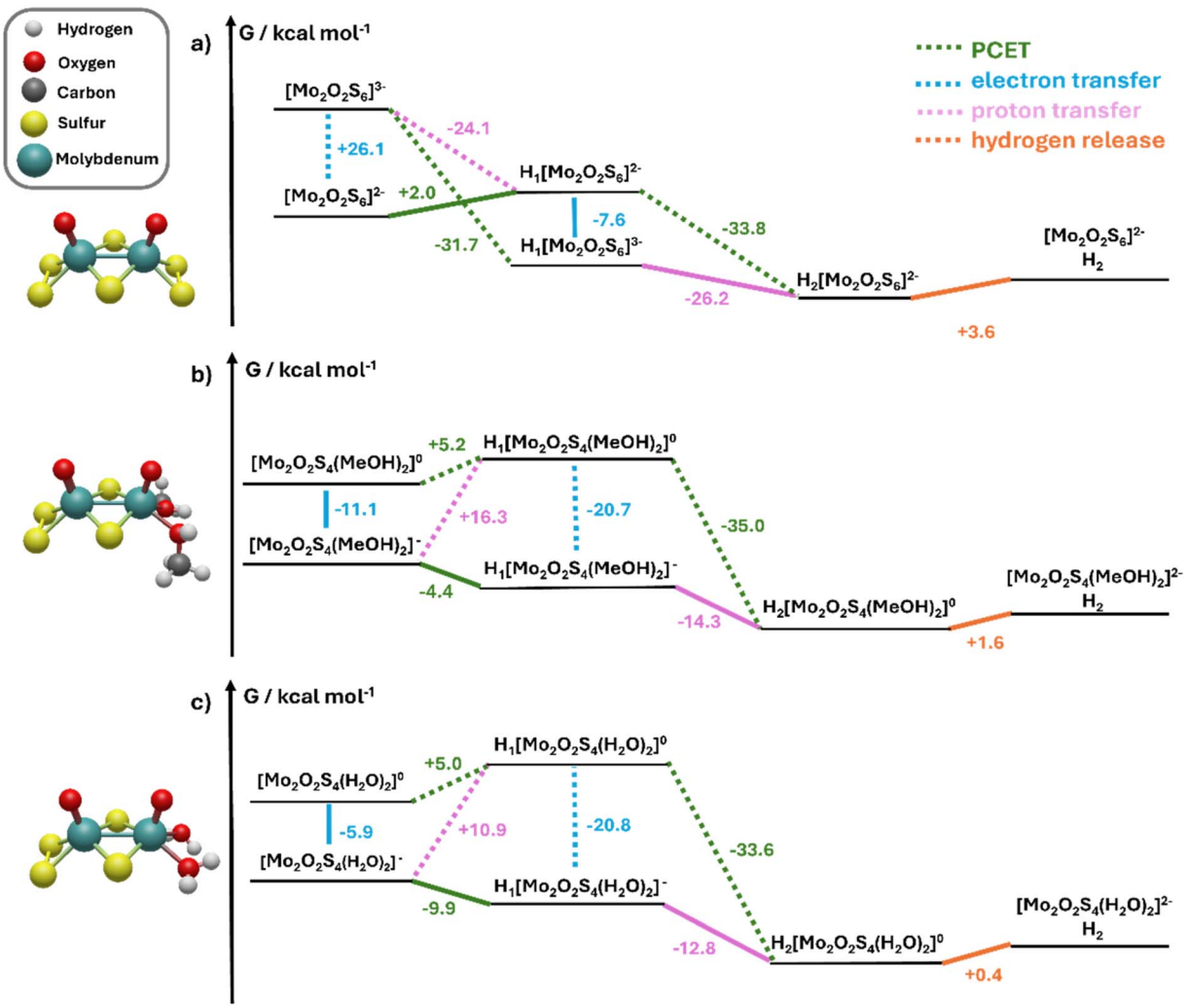

Fig. 6 Calculated Gibbs free energies (G) for structures involved in the HER process in methanol: (a) $[Mo_2O_2S_6]^{2-}$, (b) $[Mo_2O_2S_4(MeOH)_2]^0$, (c) $[Mo_2O_2S_4(H_2O)_2]^0$. Solid lines represent the favoured pathways, while dashed lines represent alternative, less favoured pathways. All calculations were performed under consideration of the underlying catalytic system (see SI).

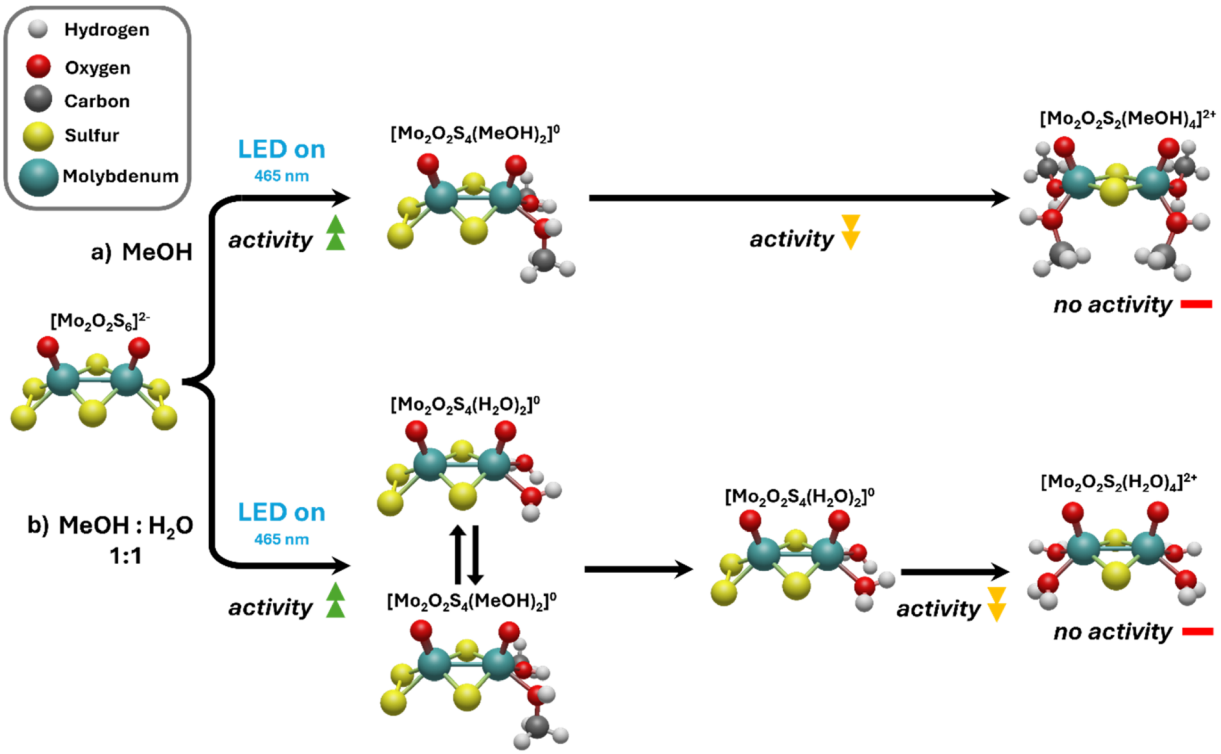

Fig. 7 Schematic illustration of the proposed ligand exchange processes of $[Mo_2O_2S_6]^{2-}$ and the respective influences on the catalyst's HER activity in (a) methanol and (b) 1 : 1 methanol–water (v/v), involving the influence of the irradiation *via* LED.

release. Hydrogen release is evaluated based on the difference in Gibbs free energy between two adsorbed hydrogen atoms (H^0) and a hydrogen molecule (H_2). In line with Sabatier's principle, the most plausible reaction pathways are expected to involve predominantly exergonic steps, moderate energy differences, and PCET steps with ΔG values near 0 kcal mol^{-1} (see Fig. 6).[24]

Based on the data presented in Fig. 6a, thermodynamically plausible reaction pathways can be identified under the previously outlined assumptions. The sequence is expected to begin with a slightly endergonic PCET step (ΔG = +2.0 kcal mol^{-1}), forming $H_1[Mo_2O_2S_6]^{2-}$. In contrast, the competing one-electron reduction pathway was calculated to be significantly more endergonic (ΔG = +26.1 kcal mol^{-1}) and is therefore thermodynamically disfavored under the applied conditions. The intermediate, $H_1[Mo_2O_2S_6]^{2-}$, is then reduced *via* an exergonic electron transfer (ΔG = −7.6 kcal mol^{-1}) followed by a strongly exergonic PT (ΔG = −26.2 kcal mol^{-1}). The resulting species, $H_2[Mo_2O_2S_6]^{2-}$, subsequently undergoes endergonic hydrogen release (ΔG = +3.6 kcal mol^{-1}). This proposed mechanism, which includes a PCET step, is in reasonable agreement with recent findings in literature.[16] However, it is important to emphasize that the pathway involves a slightly endergonic PCET step, substantial energy differences, and an endergonic hydrogen release step, deviating from the features outlined for an ideal HER processes. Notably, the performed quantum chemical calculations merely account for implicit solvent–solvate interactions. Thus, the energy of the final product $[Mo_2O_2S_6]^{2-}$ species is likely overestimated.

Two ligand exchange products which were considered in this study involve aquo or methanol ligands replacing one of the original terminal disulfide ligands, see Fig. 6b and c. The products of two ligand exchange processes with either solvent are considered to possess no HER active sites. Based on the criteria for identifying favorable reaction pathways, both ligand exchange products show similar sequences. In contrast to the parent catalyst (Fig. 6a), both reaction pathways are expected to begin with an exergonic electron transfer (b: ΔG = −11.1 kcal mol; *c*: ΔG = −5.9 kcal mol^{-1}), as the rivaling reaction pathway is an endergonic PCET (b: ΔG = +5.2 kcal mol; *c*: ΔG = +5.0 kcal mol^{-1}. This reduction is then followed by an exergonic PCET step (b: ΔG = −4.4 kcal mol; *c*: ΔG = −9.9 kcal mol^{-1}), and an exergonic PT (b: ΔG = −14.3 kcal mol; *c*: ΔG = −12.8 kcal mol^{-1}). In both cases, the final step is a slightly endergonic hydrogen release (b: ΔG = +1.6 kcal mol; *c*: ΔG = +0.4 kcal mol^{-1}). However, the product species is likely stabilized by explicit solvent effects, *i.e.*, hydrogen bonds, which were not accounted for by the current computational approach.

A direct comparison with the unmodified catalyst, $[Mo_2O_2S_6]^{2-}$, reveals notable differences. First, the pathways for the ligand-exchanged species (Fig. 6b and c) follow a different overall mechanism than that of the parent compound (Fig. 6a), and they exhibit smaller energy differences between steps. Additionally, the HER pathways of $[Mo_2O_2S_4(MeOH)_2]$ and $[Mo_2O_2S_4(H_2O)_2]$ involve only one slightly endergonic step, being hydrogen release, whereas the pathway for $[Mo_2O_2S_6]^{2-}$ includes two endergonic steps, with the hydrogen release

posing a significantly higher energy barrier. In this context, the ligand-exchanged species is proposed to undergo an initial reduction step prior to PCET, whereas the unmodified $[Mo_2O_2S_6]^{2-}$ catalyst is expected to initiate the process *via* PCET. This behavior is consistent with their respective charge states as the neutral ligand-exchanged species is more prone to reduction than the doubly negatively charged parent complex. Although the precise contribution of each individual step as well as their exact influence on overall hydrogen evolution remains difficult to quantify, these findings suggest improved catalytic properties upon ligand exchange with methanol or water. Moreover, these findings highlight the dynamic structural and electronic transformations occurring under catalytic conditions in both solvents. Notably, this trend parallels previously reported observations for $[Mo_3S_{13}]^{2-}$.

Conclusion

Raman spectroscopy, quantum chemical simulations, UV-Vis spectroscopy and gas chromatography were combined to elucidate key processes occurring during catalytic hydrogen evolution using $[Mo_2O_2S_6]^{2-}$. In particular, light-induced ligand exchange processes were proposed to play a crucial role in the activation of the catalytic cycle. The collected data allowed the development of a proposed overall mechanistic pathway and the connection to HER activity, as illustrated in Fig. 7.

Based on the findings of the catalytic activity measurements, it is evident that HER catalysis is significantly more efficient in pure methanol compared to aqueous environments.

Raman spectroscopic monitoring of the catalyst solutions suggests that for $[Mo_2O_2S_6]^{2-}$, an initial ligand exchange, where one disulfide ligand is replaced by two methanol or water ligands, occurs rapidly. UV-Vis spectroscopic investigation shows that this ligand-exchange is however mainly light-induced. Both computational and experimental findings indicate that the resulting partially substituted species is more catalytically active than the original complex. This finding supports the proposal of distinct mechanistic pathways for catalysis in methanol (Fig. 7a) and in aqueous solution (Fig. 7b).

Conflicts of interest

There are no conflicts to declare.

Data availability

Data for this article, including experimental, analytical, catalytic and computational data are available at https://zenodo.org at https://doi.org/10.5281/zenodo.18267196.

Acknowledgements

The authors gratefully acknowledge the Deutsche Forschungsgemeinschaft DFG (TRR 234 "CataLight", project no: 364549901, projects A04, A05, C02) and the Top-Level Research Area "SusInnoScience (Mainz) for financial support. S.H.K. gratefully acknowledges the HaVo Stiftung for a PhD fellowship.

References

1 M. Heiland, R. De, S. Rau, B. Dietzek-Ivansic and C. Streb, *Chem. Commun.*, 2022, **58**, 4603–4606.
2 M. L. Grutza, A. Rajagopal, C. Streb and P. Kurz, *Sustain. Energy Fuels*, 2018, **2**, 1893–1904.
3 W. Hu, L. Xie, C. Gu, W. Zheng, Y. Tu, H. Yu, B. Huang and L. Wang, *Coord. Chem. Rev.*, 2024, **506**, 215715.
4 Y. Lei, M. Yang, J. Hou, F. Wang, E. Cui, C. Kong, S. Min and R. Li, *Chem. Commun.*, 2018, **54**, 603–606.
5 S. Batool, M. Langer, S. N. Myakala, M. Heiland, D. Eder, C. Streb and A. Cherevan, *Adv. Mater.*, 2024, **36**, 2305730.
6 A. Rajagopal, F. Venter, T. Jacob, L. Petermann, S. Rau, S. Tschierlei and C. Streb, *Sustain. Energy Fuels*, 2019, **3**, 92–95.
7 M. Dave, A. Rajagopal, M. Damm-Ruttensperger, B. Schwarz, F. Nägele, L. Daccache, D. Fantauzzi, T. Jacob and C. Streb, *Sustain. Energy Fuels*, 2018, **2**, 1020–1026.
8 Y. Lei, M. Yang, J. Hou, F. Wang, E. Cui, C. Kong and S. Min, *Chem. Commun.*, 2018, **54**, 603–606.
9 A. Baloglou, M. Ončák, M. L. Grutza, C. Van Der Linde, P. Kurz and M. K. Beyer, *J. Phys. Chem. C*, 2019, **123**, 8177–8186.
10 T. Wang, J. Zhuo, K. Du, B. Chen, Z. Zhu, Y. Shao, M. Li, T. Y. Wang, J. Q. Zhuo, K. Z. Du, B. B. Chen, Z. W. Zhu, Y. H. Shao and M. X. Li, *Adv. Mater.*, 2014, **26**, 3761–3766.
11 J. D. Benck, T. R. Hellstern, J. Kibsgaard, P. Chakthranont and T. F. Jaramillo, *ACS Catal.*, 2014, **4**, 3957–3971.
12 S. H. Kolbinger, L. Haxha, P. C. Schröder, D. Kowalczyk, L. Senz, L. Schleicher, A. Mukherjee, D. Malcolm, C. L. Kufner, D. Ziegenbalg and C. Streb, *Sustain. Energy Fuels*, 2026, **10**, 1313–1320.
13 S. Batool, S. P. Nandan, S. N. Myakala, A. Rajagopal, J. S. Schubert, P. Ayala, S. Naghdi, H. Saito, J. Bernardi, C. Streb, A. Cherevan and D. Eder, *ACS Catal.*, 2022, **12**, 6641–6650.
14 B. Seo, G. Y. Jung, S. J. Lee, D. S. Baek, Y. J. Sa, H. W. Ban, J. S. Son, K. Park, S. K. Kwak and S. H. Joo, *ACS Catal.*, 2020, **10**, 652–662.
15 B. Keita, S. Floquet, J.-F. Lemonnier, E. Cadot, A. Kachmar, M. Bénard, M.-M. Rohmer and L. Nadjo, *J. Phys. Chem. C*, 2008, **112**, 1109–1114.
16 J. McAllister, N. A. G. Bandeira, J. C. McGlynn, A. Y. Ganin, Y. F. Song, C. Bo and H. N. Miras, *Nat. Commun.*, 2019, **10**, 370.
17 Z. Huang, W. Luo, L. Ma, M. Yu, X. Ren, M. He, S. Polen, K. Click, B. Garrett, J. Lu, K. Amine, C. Hadad, W. Chen, A. Asthagiri and Y. Wu, *Angew. Chem., Int. Ed.*, 2015, **54**, 15181–15185.
18 A. Müller, E. Diemann, R. Jostes and H. Bögge, *Angew Chem. Int. Ed. Engl.*, 1981, **20**, 934–955.
19 D. Kowalczyk, P. Li, A. Abbas, J. Eichhorn, P. Buday, M. Heiland, A. Pannwitz, F. H. Schacher, W. Weigand, C. Streb and D. Ziegenbalg, *ChemPhotoChem*, 2022, **6**, e202200044.
20 A. Vaidyalingam and P. K. Dutta, *Anal. Chem.*, 2000, **72**, 5219–5224.

21 E. Villani, K. Sakanoue, Y. Einaga, S. Inagi and A. Fiorani, *J. Electroanal. Chem.*, 2022, **921**, 116677.
22 E. Deponti, A. Luisa, M. Natali, E. Iengo and F. Scandola, *Dalton Trans.*, 2014, **43**, 16345.
23 M. P. Mclaughlin, T. M. Mccormick, R. Eisenberg and P. L. Holland, *Chem. Commun.*, 2011, **47**, 7989.
24 H. Ooka, J. Huang and K. S. Exner, *Front. Energy Res.*, 2021, **9**, 654460.